



## Microporous and Mesoporous Activated Carbons from Tea Stalk and Tea Stalk Pulps: Effect of Lignin Removal by One-Step and Two-Step Organosolv Treatment

Sibel Başakçılardan Kabakcı<sup>1\*</sup> , Basak Karakurt Cevik<sup>1</sup> , Gamze Sultan Bas Berkem<sup>2</sup> 

<sup>1</sup>Energy Systems Engineering Department, Faculty of Engineering, Yalova University, Türkiye.

<sup>2</sup>Polymer Materials Engineering Department, Faculty of Engineering, Yalova University, Türkiye.

**Abstract:** Delignification is a crucial pretreatment in the production of diverse value-added products from lignocellulosics. While modifying the surface functional groups, delignification also increases the specific surface area by providing a porous structure to the lignocellulosic biomass. Hydrothermal pretreatment can be used prior to delignification, to recover hemicellulose and boost delignification. By removing lignin and hemicellulose, cellulose-rich pulp becomes more accessible for activation. In the present study, three different activated carbons were prepared: activated carbon from tea stalk itself (ATS), activated carbon from tea stalk pulp obtained by using glycerol organosolv pretreatment (ATP), activated carbon from tea stalk hydrochar pulp obtained by using sequential hydrothermal pretreatment-organosolv delignification (AHTP). Each precursor was carbonized (at 800 °C) in the presence of KOH (KOH/precursor: 2/1). Activated carbons were characterized for their elemental content, surface functional groups, thermal stability, crystallinity, surface morphology, surface area and porous structure using elemental analysis (C-H-N-S), FTIR, TGA, XRD, SEM and, BET analysis, respectively. While hydrothermal pretreatment prior to organosolv pulping reduced the delignification yield, it also altered the pore structure of activated carbon. Among the activated carbons, only ATS had microporous structure with an average pore radius of 1 nm. ATP had the highest surface area (2056.72 m<sup>2</sup>/g) and micropore volume (0.81 cm<sup>3</sup>/g). Having mesopores (with an average pore radius of 5.74 nm) in its structure, AHTP had the least micropore volume (0.464 cm<sup>3</sup>/g) and surface area (1179.71 m<sup>2</sup>/g). The presence of micro and mesopores broadens the potential applications of activated carbon ranging from environmental applications to energy storage.

**Keywords:** Activated carbon, alkaline-glycerol organosolv treatment, hydrothermal pretreatment.

**Submitted:** September 19, 2023. **Accepted:** November 8, 2023.

**Cite this:** Başakçılardan Kabakcı S, Karakurt Cevik B, Bas Berkem GS. Microporous and Mesoporous Activated Carbons from Tea Stalk and Tea Stalk Pulps: Effect of Lignin Removal by One-Step and Two-Step Organosolv Treatment. JOTCSA. 2024;11(1):171-88.

**DOI:** <https://doi.org/10.18596/jotcsa.1362724>

**\*Corresponding author's E-mail:** [sibel.kabakci@yalova.edu.tr](mailto:sibel.kabakci@yalova.edu.tr)

### 1. INTRODUCTION

Activated carbons are carbon-rich porous materials which are prepared from different resources such as coal, coke, peat and biomass. Having the highest share of lignocellulosic biomass, agricultural wastes and residues are sustainable raw materials to produce value-added products such as activated carbon (1-3). Several lignocellulosic feedstocks have been preferred as precursors such as pineapple leaf and coconut shell (4), kenaf and rapeseed (5), corn straw (6), oil palm

leaves (7), olive bagasse (8), cherry stones (9), almond shell wastes (10). Due to their high surface area, variable porosity and surface functional groups, activated carbons are used as adsorbents for the removal of water pollutants and air pollutants, as catalyst support for preparing catalyst, as electrodes in supercapacitors for storing ions, and as carbon nanotubes and carbon fiber.

The volume and diameter of pores, surface area, micropore volume and surface functional groups of

activated carbon are affected from the activating agent, activation type (physical or chemical), activation conditions, carbonization conditions, and the lignocellulosic precursor (11-13). The structural components of lignocellulose (namely cellulose, hemicellulose and lignin) have great impact on both yield and porous structure of activated carbon mainly due to their different chemical structure and thermal stability (14-17). In the study of Guo and Rockstraw (18), activated carbons of xylan, cellulose and lignin had different pore structures at same activation conditions. Lignin is the major component that contributes to the activated carbon yield, while cellulose, lignin and hemicellulose alter the porous structure (19, 20). Specific surface area and porosity of the activated carbon are higher as the precursor has high cellulose content (4). To take advantage of the high cellulose content, biomass can be partially delignified prior to activation/carbonization (6, 21-23). Chen et al. (6) fractionated cellulose, hemicellulose and lignin using NaOH and urea solution. Then, activated carbon samples were obtained by carbonizing those fractions under N<sub>2</sub> atmosphere at 800 °C in the presence of NaOH. Their study showed that activated carbon obtained from cellulosic fraction has better properties than activated carbon obtained from the lignocellulosic biomass itself. Mittal et al. (24) separated the cellulosic fraction by pretreating rice straw with an alkaline ionic liquid (choline hydroxide). The cellulosic fraction was carbonized at 600 °C for 3 hours under an argon atmosphere. In this study, adsorption capacity of mesoporous cellulose-based activated carbon was high. Han et al. (25) pre-treated poplar wood using CH<sub>3</sub>COOH and NaClO<sub>2</sub> solution at 80 °C for 18 hours. The cellulose-rich fraction was carbonized at 1000 °C for 2 h (under argon atmosphere). It was observed that the pore size of the pretreated activated carbon was lower than the activated carbon obtained from poplar wood. Sun and Hong (26) used different cellulose-based polymers ( $\alpha$ -cellulose, methyl cellulose, hydroxyethyl cellulose and cellulose acetate) as a precursor. First, the samples were carbonized under Ar atmosphere (at 400 or 500 °C), and then under CO<sub>2</sub> atmosphere for 2 h. Based on experimental results, the difference in functional groups in the cellulose samples not only affects the pore structure, but also improves the adsorption properties. As can be seen from the studies summarized above, activated carbons obtained from cellulose-rich precursors are better due to properties such as pore structure, pore size, surface area of activated carbon, and versatile surface functional groups.

One way to obtain cellulose-rich precursors is to delignify the biomass. There are various physico-chemical pretreatment methods for the delignification of lignocellulosic biomass such as acid pretreatment, NaOH pretreatment, ammonia pretreatment, organosolv pretreatment, ionic liquid pretreatment, deep eutectic solvent pretreatment (27). Among them, organosolv pretreatment has the advantage of lignin

recovery while enriching cellulose in the pulp. In the organosolv treatment, lignocellulosic biomass is brought into contact with a solvent in the presence of a catalyst (28). This process can be carried out under pressure, or it can be carried out at atmospheric pressure at relatively higher temperatures. The type of solvent and biomass, particle size of the biomass, biomass/solvent ratio, pretreatment conditions (temperature, pressure, mixing speed, time) affect the extent of delignification (29). The cellulose-rich fraction is separated from the solution by filtration. Lignin is precipitated by diluting the organosolv solution with water. Solvent recovery is often attempted from the solution if the solvent has low boiling point temperature (30). Sometimes hydrothermal pretreatment is applied prior to organosolv pulping to recover the hemicellulose sugars, to increase the accessibility of enzymes to cellulose and to boost delignification (31-35). Hydrothermal pretreatment, which is a simple and low-cost method, uses water as a solvent and pretreatment is carried out at temperatures between 160-230 °C (36). In this method, where most of the hemicellulose is degraded, swelling and partial hydrolysis of cellulose and partial decomposition and repolymerization of lignin are observed depending on the conditions of the hydrothermal pretreatment (37). After hydrothermal pretreatment, the liquid fraction containing a high percentage of sugar can be converted into platform chemicals using different conversion methods (38). The solid fraction, which is named as hydrochar, can be used as an adsorbent for environmental applications, a solid fuel for the production of energy or energy carriers (such as syngas), a precursor for the preparation of activated carbon or can be further processed to produce high value-added products (39, 40).

There are many studies in the literature that focuses on using cellulose, microcrystalline cellulose, or cellulose-rich biomass as precursors for activated carbon preparation. Studies which use cellulose-rich pulp from organosolv treatment as a precursor are very rare. Unlike the others, in this study, delignification of lignocellulosic biomass was done by a single-stage glycerol-organosolv treatment and a sequential hydrothermal pretreatment-organosolv treatment separately. Cellulose-rich pulps obtained by both methods and the tea stalk itself were used as precursors to produce microporous-mesoporous activated carbon. Activated carbons are compared based on their properties and potential end-uses were discussed.

## 2. EXPERIMENTAL SECTION

### 2.1. Materials

Tea stalk samples were supplied from a tea processing factory. All tea stalk samples were dried (105 °C for 24 h) before analyses and pretreatments to prevent samples from rotting and to provide better conditions for

storage. After grinding, samples were sieved by using RESTCH AS 200 vibrating sieve to have a uniform particle size (250  $\mu\text{m}$ ). Dry tea stalk samples with uniform particle size are named as TS.

Chemicals including glycerol, NaOH and  $\text{H}_2\text{SO}_4$  were of analytical grade and used without further purification.

## 2.2. Methods

### 2.2.1. Hydrothermal pretreatment

Hydrothermal pretreatment of TS was carried out in a 250 mL non-stirred, temperature-controlled, stainless-steel batch reactor. Hydrothermal pretreatment conditions were selected based on our previous study (pretreatment temperature: 220  $^{\circ}\text{C}$ , residence time: 90 min, tea stalk/water ratio: 1 g/4 mL) (41). After pretreatment, the reactor was cooled rapidly by using ice bath. Gases, which formed during the pretreatment were not collected. The mixture was filtered to separate hydrochar. The hydrochar of TS samples (named as HTS) were washed with deionized water and then dried in an oven at 105  $^{\circ}\text{C}$  for 24 h.

HTS samples were delignified by using alkaline glycerol organosolv treatment as explained below. The pulp obtained after sequential hydrothermal pretreatment and organosolv treatment was named as HTP.

### 2.2.2. Alkaline-glycerol organosolv treatment

Alkaline-glycerol organosolv method, which we previously used for delignification (42), was modified in this study to increase the lignin yield. 20 g tea stalk, 50

mL of 0.4 M NaOH solution and 150 mL glycerol were mixed in a three-necked glass reactor equipped with a reflux condenser and a thermocouple. First, the mixture was mixed for 30 min at 90  $^{\circ}\text{C}$ , then the temperature was raised to 115  $^{\circ}\text{C}$ . The mixture was continuously mixed for 90 min at this temperature. At the end of the treatment, pulp was separated from the liquor, and washed with hot water (water at 55  $^{\circ}\text{C}$ ) and then dried in an oven at 100  $^{\circ}\text{C}$  for 24 h. The pulp obtained after organosolv pretreatment was named as TP.

To precipitate the lignin, filtrate was diluted with deionized water to 1L (at 55  $^{\circ}\text{C}$ ) and the pH was decreased to 2-2.5 by using 0.1 M  $\text{H}_2\text{SO}_4$ . After precipitation, lignin was separated, washed with water and then dried. Characteristics of lignins are not given as they are beyond the scope of this article.

### 2.2.3. Preparation of activated carbon

Dry TS, TP and HTP samples were mixed with KOH at a ratio of 1:2 (wt:wt). After gently mixing KOH with the sample, the mixture in a ceramic boat was placed in a horizontal tubular furnace. The sample was heated at a heating rate of 10  $^{\circ}\text{C}/\text{min}$  up to 800  $^{\circ}\text{C}$  and kept at this temperature for 1h. During heating and cooling, tubular furnace was continuously flushed with nitrogen gas. After activation, samples were washed with 0.1 M HCl and deionized water. Then, the samples were dried at 105  $^{\circ}\text{C}$  for 24 h. Activated carbons obtained from TS, TP and HTP were named as ATS, ATP and AHTP respectively. Block diagrams regarding the preparation of ATS, ATP and AHTP are given in Figure 1.

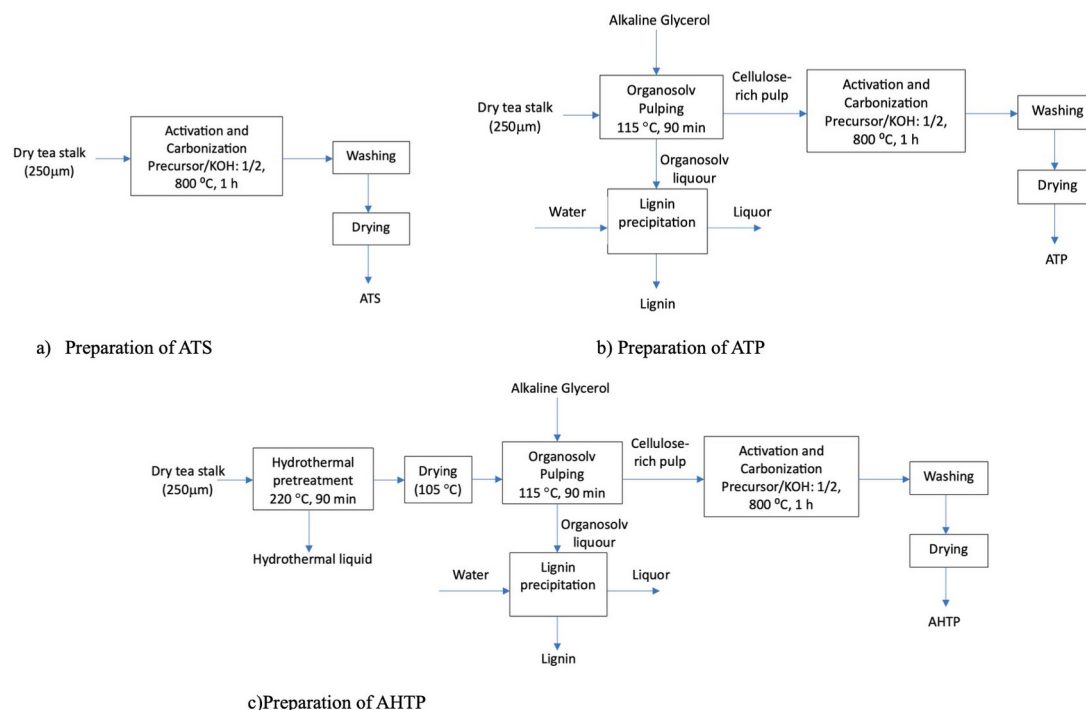


**Figure 1:** Preparation procedure and naming of the activated carbons.

## 2.3. Analyses

Proximate analyses of TS, HTS, TP and HTP were done using thermogravimetry method as described in Garcia,

Pizarro (43). The elemental analysis of TS, HTS, TP, HTP, ATS, ATP and AHTP were carried by an elemental analyzer (LECO, CHNS-932). Acid-insoluble lignin content of TS, TP and HTP was determined by using gravimetric method as described in NREL/TP-510-42618 (44). Holocellulose content of TS was determined as explained in Salim et al. (45).

Fourier Transform Infrared (FTIR) spectra of TS, HTS, TP, HTP, ATS, ATP and AHTP were obtained using a spectrometer (Perkin Elmer Spectrum 100) coupled with a universal attenuated total reflectance (ATR) sampling device with a diamond crystal. The spectra were recorded with a resolution of 4 1/cm, in the range from 400 to 4000 1/cm.

For thermal stability, thermogravimetric analyzer (Seiko, TG/DTA 6300) was used. Samples were heated from room temperature to 900 °C with a heating rate of 40 °C/min and maintained for 7 min.

Surface morphologies of HTS, ATS, ATP and AHTP were investigated by FEI Inc., Inspect S50 SEM. Samples were investigated under 20 kV in the high vacuum mode using secondary electrons with different magnifications.

The surface area and pore structure characteristics of ATS, ATP and AHTP were determined by using Quantachrome-Autosorb iQ BET analyzer at 77K in the relative pressure range of 0.001 and 0.99. Before analysis, samples were degassed at 180 °C for 24 h.

The XRD patterns of ATS, ATP and AHTP were collected using Rigaku Smartlab X-Ray diffractometer, operating at 40kV and 30 mA, with a scan range of 10 to 80 °, a step width of 0.02° and a scan speed of 1.0039 °/min.

### 3. RESULTS AND DISCUSSION

#### 3.1. Characterization

The proximate analysis (volatile matter, fixed carbon and ash content) and ultimate analysis (C, H, N and S content) of TS, HTS, TP, HTP, ATS, ATP and AHTP are presented in Table 1. Tea stalk is a lignin-rich lignocellulosic biomass, which contains 33.9±1.1 % lignin and 49.2±1.3 holocellulose in its structure.

During hydrothermal pretreatment, biomass undergoes several reactions including hydrolysis, dehydration, decarboxylation, condensation, and polymerization (40). The extent of the reactions, which determines the hydrochar yield (mass ratio of hydrochar to biomass on dry weight basis), depend on the hydrothermal conditions and the type of biomass (especially lignin, cellulose and hemicellulose content). After hydrothermal pretreatment of TS, the hydrochar yield was calculated as 70.7±0.3 %. Due to the high lignin content of TS and moderate pretreatment temperature (220 °C), this hydrochar yield was expected as explained briefly in Gulec et al. (46).

After hydrothermal pretreatment, the volatile matter content of the tea stalk increased, the fixed carbon content decreased, and consequently the carbon content increased by 3%. Hydrothermal pretreatment also reduced the ash content of the TS by 5.3%.

Alkaline-glycerol organosolv pretreatment is an effective delignification method (28). When alkaline-glycerol organosolv treatment was applied directly to TS, 7.1±0.2 % lignin (acid-insoluble lignin) was detected in TP, showing that some of the lignin retained in the pulp. In the case of sequential hydrothermal pretreatment and organosolv treatment, the lignin content in HTP was 11.6±0.7 %. Based on acid-soluble lignin content, hydrothermal pretreatment prior to glycerol organosolv treatment reduced delignification.

The application of hydrothermal pretreatment before the organosolv treatment affected the pulp content. The carbon content of TP and HTP was close to each other (37.8% and 36.9%, respectively) and a small part of this carbon is fixed carbon. Cellulose-rich TP and HTP were found to have a lower carbon content than the average carbon content of a typical cellulose (44.06 %), and a higher fixed carbon content than a typical cellulose (4.35 %) (47). Since delignification was not 100% in both treatments, there was still lignin in both TP and HTP. The high fixed carbon content of TP and HTP can be explained by the high fixed carbon content of the residual lignin (23.09 %) (47).

**Table 1:** Proximate and ultimate analysis of TS, HTS, TP, HTP, ATS, ATP and AHTP.

	TS	HTS	TP	HTP	ATS	ATP	AHTP
<b>Proximate analysis (wt.%, db.)</b>							
VM	71.1	72.6	91.4	92.3	n.d.	n.d.	n.d.
FC	25.1	23.8	6.9	6	n.d.	n.d.	n.d.
Ash	3.8	3.6	1.7	1.7	n.d.	n.d.	n.d.
<b>Ultimate analysis (wt.%, db.)</b>							
C	46.6	48	37.8	36.9	61.3	56.3	52.3
H	5.5	5.4	8.3	8	0.5	0.2	0.2
N	2.6	2.3	0.5	0.6	1.1	0.5	0.4
S	0.1	0	0	0	0	0	0

VM: Volatile matter, FC: Fixed carbon, A: Ash, db: dried basis

\* Proximate and ultimate analyses were done twice. Mean values were given in Table 1.

After activation-carbonization, the carbon content of TS, TP and HTP increased by 31.5%, 49% and 41.7%, respectively. Based on elemental analysis results, the oxygen content of ATP and AHTP was high. This was mainly due to high oxygen content of TP (51.7%) and HTP (52.8%). Not hydrothermal pretreatment but delignification definitely increased the oxygen content of the pulps. The oxygen-rich functional groups of TP, HTP, ATP and AHTP were also supported by the FTIR spectra.

### 3.2. Thermal Stability of TS, HTS, TP and HTP

Thermal stability is an important property of all bio-based materials. Figure 2 shows the TG and DTG curves of TS, HTS, TP and HTP. The thermogravimetric curve of TS showed a thermal degradation curve of a typical biomass. Moisture removal was observed in the first stage at temperatures between 25 °C and 110 °C. The thermal degradation of structural components (hemicellulose, cellulose and lignin) was seen at temperatures between 120 °C and 600 °C.

Like TS, the thermal degradation of HTS occurred in two stages at a wide temperature range. Hydrochar has a more stable structure compared to biomass since hemicellulose is partially degraded and light volatiles leave the structure during hydrothermal treatment. HTS was also more thermally stable than TS. Better thermal stability of the structure was also supported by the shifting of  $T_{max}$  (the temperature at which the mass loss

rate is maximum) from 337 °C to 344 °C after hydrothermal treatment.

While the thermal degradation of pure cellulose takes place in two stages (the first step is moisture removal), the thermal degradation of TP and HTP differs slightly from the typical thermogram of cellulose. This is because although it is rich in cellulose, there is some lignin in the pulp and chemical treatment of the cellulose disrupts the structure (48). Studies investigating the effects of chemical treatment on cellulose structure have shown that the thermal degradation of cellulose occurs in three stages, and the thermal degradation after moisture removal is between 110 °C – 285 °C and 288 °C – 600 °C (49, 50). In the present study, thermal degradation of both TP and HTP occurred in three steps. The mass loss in the first stage in both samples was due to the removal of moisture. The degradation of TP in the second stage was between 180 °C and 235 °C, with a  $T_{max}$  of 220 °C. The mass loss of TP in the third stage was between 280 °C and 344 °C, and the highest mass loss rate in this stage was seen at 322 °C.

The thermal degradation of HTP started with the removal of moisture. The second degradation was between 172 °C and 236 °C, with a  $T_{max}$  of 221 °C. The third stage of thermal degradation was observed at temperatures between 290 °C and 344 °C. At this stage, the temperature with the highest mass loss rate was determined as 327 °C. Application of hydrothermal pretreatment before the organosolv treatment slightly increased the thermal stability of the pulp.

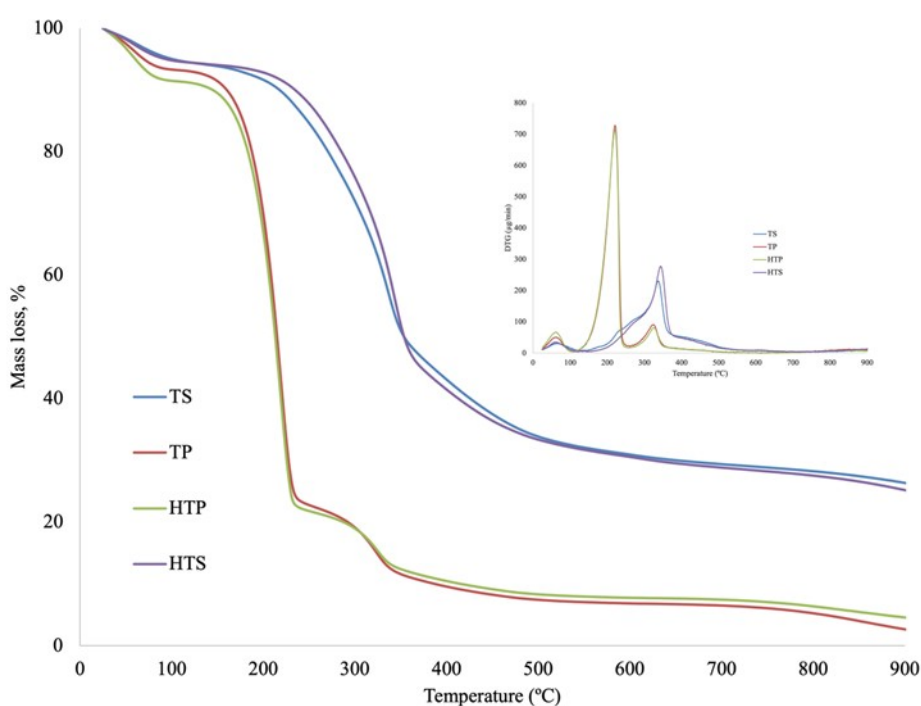


Figure 2: TG curves of TS, HTS, TP and HTP.

### 3.3. FTIR Analysis

The FTIR spectra of TS, HTS, TP and HTP are shown in Figure 3. Tea stalk has a broad peak at 3000-3800 1/cm (centered at 3338 1/cm) due to -OH stretching vibration in the hydroxyl functional groups (in compounds such as phenolics, aliphatic alcohols, carboxylic acids etc.) (51). The peaks at 2917 1/cm and 2849 1/cm correspond to stretching vibration of aliphatic C-H bond in  $-CH_2-$  structures (52). The peaks appearing between 2009-2160 1/cm originate from the stretching vibration of allene ( $C=C=C$ ) and ketamine ( $C=C=N$ ) groups in tea stalk (51, 53, 54). Stretching vibration of  $C=C$  bond in aromatic rings and C-H stretching appear at 1515 1/cm and 1362 1/cm. HTS has a similar FTIR spectra with that of TS. Only difference between them was the intensity of the bands of HTS at 1200-3600 1/cm region, which confirms that a degradation was observed but functional group was not changed. Compared to TS, the stretching vibration of -OH (at 3000-3600 1/cm), -CH (at 2800-3000 1/cm) and  $C=C=C$  (at 2000-2200 1/cm) in HTS structure were much lower. After hydrothermal pretreatment, the characteristic bands of lignin (1660-1638 1/cm) and (1400-1500 1/cm) were retained, with a slight decrease in intensities. Yu et al. (55) made a similar observation and concluded that the structure of

lignin was slightly changed with temperature due to the cleavage of C-C, C=C and C-H bands. The characteristic stretching vibrations of cellulose at 1000-1400 1/cm region were slightly less due to partial degradation of cellulose under hydrothermal conditions.

The effect of delignification was observable from the FTIR spectra of TP and HTP. The wide peak appearing between 3000-3600 1/cm for all samples reflect the stretching vibration of -OH group. The bands at 2880 1/cm and 2920 1/cm were assigned to -CH stretching vibration of  $-CH_2$  and  $-CH_3$  groups. The peaks at 2160 1/cm, 2040 1/cm and 2000 1/cm were attributed to  $C=C=C$  and  $C=C=N$  stretchings. While FTIR spectra of TS reflects the conjugated carbonyl stretching (at 1660-1638 1/cm) and aromatic skeleton vibration in lignin (at 1600 1/cm, 1500 1/cm and 1440 1/cm) (56, 57); the intensity of the same peaks in the FTIR spectra of both TP and HTP were comparatively very low due to delignification. In all spectra, in-plane C-H deformation (at 1360 1/cm), in-plane O-H bending in cellulose structure (at 1320 1/cm) and C-C, C-O, C=O stretch (at 1240 1/cm) were observed.

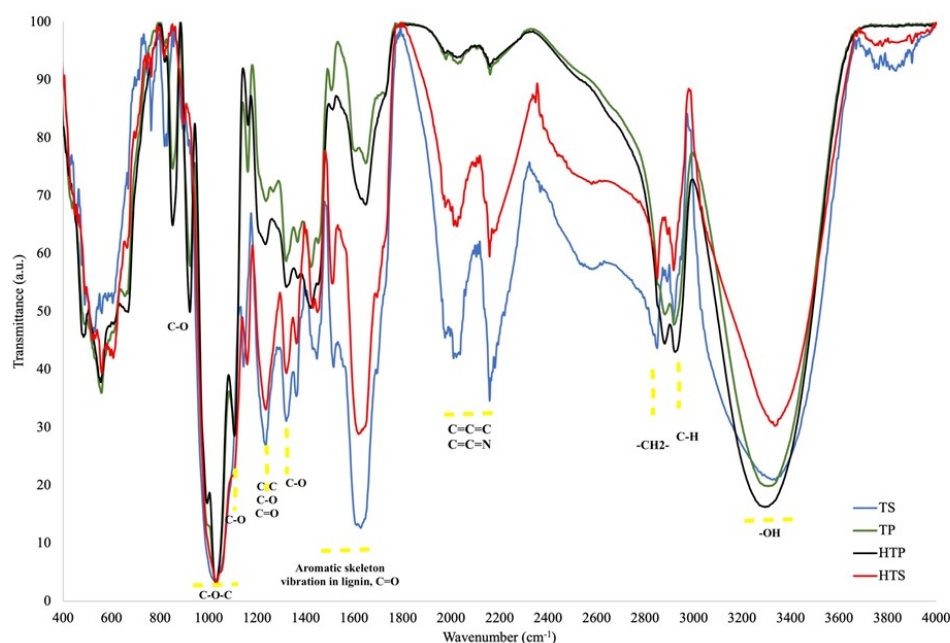


**Figure 3:** FTIR spectra of TS, HTS, TP and HTP.

Figure 4 shows the FTIR spectra of ATP, AHTP and ATS. The spectra of the activated carbons were similar, only the intensities of the vibrations altered. The stretching vibration of -OH in phenol and carboxyl groups centered at 3073 1/cm (58) was more intense in the spectra of ATS than that of ATP and AHTP. Similarly, C=O stretching vibration (in ketene groups) at 2420-2430 1/cm (59) was more intense in the spectra of ATS than that of ATP and AHTP. The spectra of all activated carbons showed the stretching vibration of  $C=C=C$  (in allene group) at 2160 1/cm (60, 61). C=O stretching

vibration of carbonyl and carboxylate groups (such as ketones, aldehydes) was observed in the spectra of all activated carbons at 1600-1700 1/cm with same intensity (62).  $C=C$  stretching vibration of aromatic rings at 1560 1/cm (51) was also detected in all spectra. C-O stretching vibration (in ethers, alcohols, acids, esters) at 1017 1/cm (63) was much more intense in the spectra of ATP. AHTP and ATS showed stronger stretching at 1200 (C-C, C-O, C=O stretching vibration). Bending vibration of C-H in the aromatic rings at 820-840 1/cm (64) was observed in the spectra of AHTP and ATS.

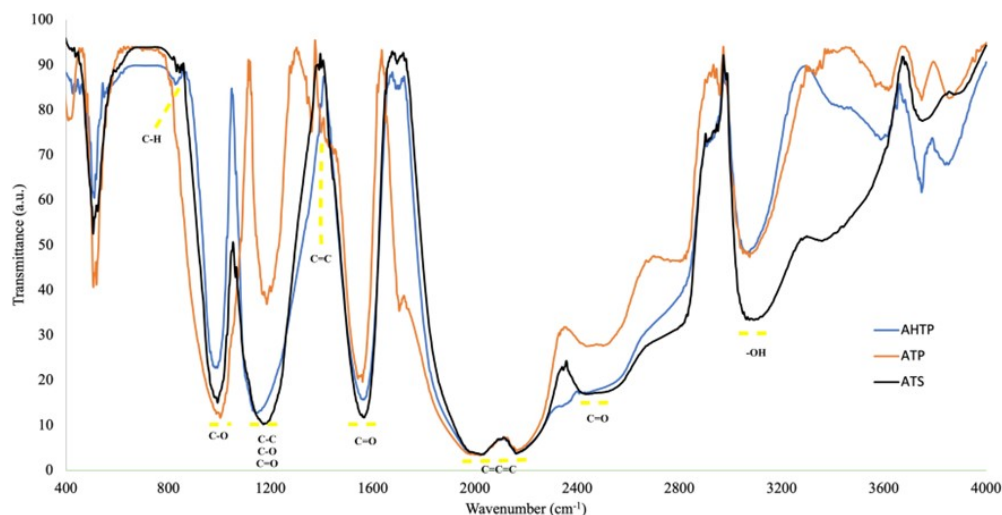


**Figure 4:** FTIR spectra of ATS, ATP and AHTP.

### 3.4. X-ray Diffraction Analysis

Depending on the type of biomass, cellulose is present in the structure as crystalline and amorphous form (65). Any pretreatment using chemicals such as acids, bases and solvents might affect the amorphous structure (66-70). In order to observe what extent the pretreatments changed the cellulose in the biomass structure, x-ray diffraction analysis was also performed on hydrochar and pulps.

XRD patterns of TP, HTP and HTS are presented in Figure 5. The XRD patterns of HTS exhibit diffraction peaks at  $15^\circ$  (101),  $22^\circ$  (002) and  $34.5^\circ$  (040), which indicates that both amorphous and crystalline cellulose structure was preserved during hydrothermal pretreatment (64). A similar result was observed by Fan et al. (71), who studied the hydrothermal carbonization

of Chinese fan palm leaves at different temperatures. In the study of Fan et al. (72), a broad peak between  $15^\circ$  and  $16^\circ$ , which indicated amorphous structure, was observed in the XRD of hydrochars obtained at 180 and  $220^\circ\text{C}$ , while this structure was not seen above  $260^\circ\text{C}$ . In the x-ray diffractions of TP and HTP obtained by organosolv pretreatment and sequential hydrothermal-organosolv pretreatments, only broad peaks at  $22^\circ$  (002 plane) and  $34.5^\circ$  were observed. Alkaline-glycerol organosolv pretreatment completely removed the amorphous structure. Sun et al. (72), who applied glycerol organosolv treatment to wheat straw, showed that the amorphous structure (amorphous cellulose, lignin and hemicellulose) decreased (hence the crystal index increased) and the average crystal size of cellulose decreased.

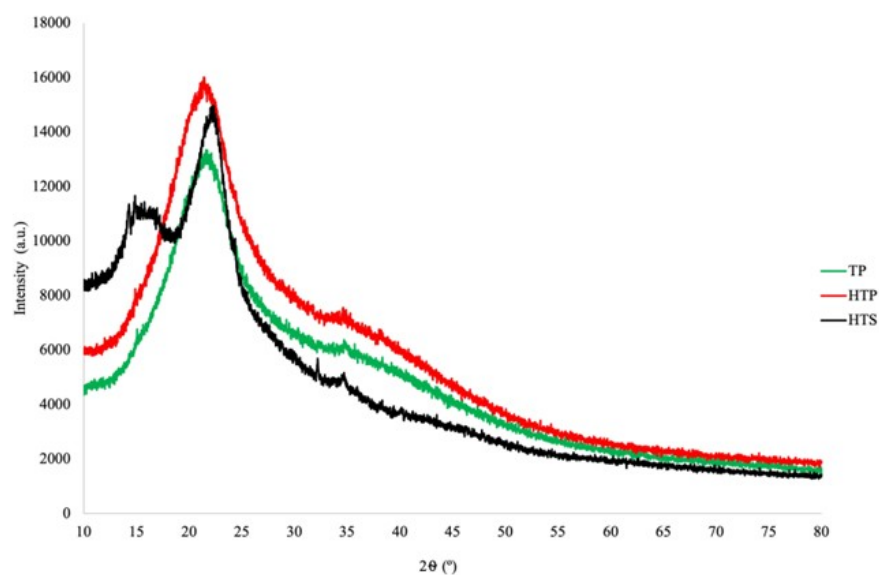


**Figure 5:** X-ray diffraction patterns of TP, HTP and HTS.

After carbonization and activation, a broad hump (indicating the amorphous graphitic carbon) between  $17^\circ$  and  $35^\circ$  was observed in the x-ray diffraction pattern of ATP, ATS and AHTP (73). A weaker and

broader hump at  $41-47^\circ$  was also observable in all patterns, which is also a characteristic diffraction of amorphous graphite structure (74). Unlike ATP and ATS, AHTP shows sharp diffraction peaks of graphitic carbon

at  $2\theta=20^\circ, 26^\circ, 36^\circ, 41^\circ, 44^\circ, 47.5^\circ, 52^\circ, 53.5^\circ, 55.5^\circ, 63^\circ$  (55, 75). Obviously, AHTP has higher crystallinity compared to ATP and ATS.

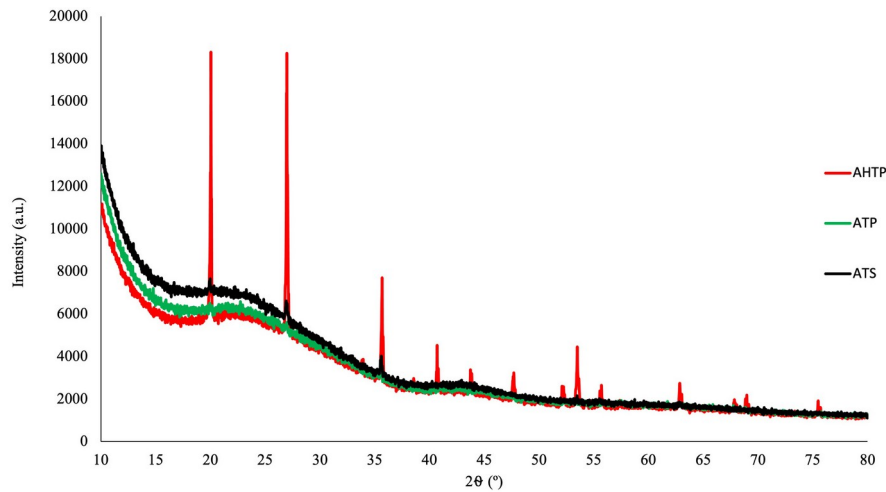


**Figure 6:** X-ray diffraction pattern of AHTP, ATP and ATS.

### 3.5. SEM Analysis

SEM provides micrographs that show surface morphology. The surface morphologies of HTS, ATS, ATP and AHTP can be seen in Figure 7. HTS shows an irregular and rough surface. The formation of microspheres or pores was not observed on the surface of HTS, showing that hydrothermal treatment temperature ( $220^\circ\text{C}$ ) was not able to destruct lignocellulosic structure (76). The SEM image of ATS shows a dense porous structure with many three-dimensional channels. Activation of tea stalk with KOH resulted in well-developed micropores on the surface of

the ATS. Although the SEM image of ATP was densely microporous like that of ATS, the presence of mesopores was noteworthy. Removal of lignin from the lignocellulosic structure leads pore formation. Therefore, mesopores in ATP were due to severe destruction of lignocellulosic structure by organosolv delignification, which was done prior to activation. AHTP images also show the porous structure with a wider range of pores compared to that of ATP. Both hydrothermal pretreatment and organosolv delignification corroded the lignocellulosic structure, which resulted in mesopore formation.

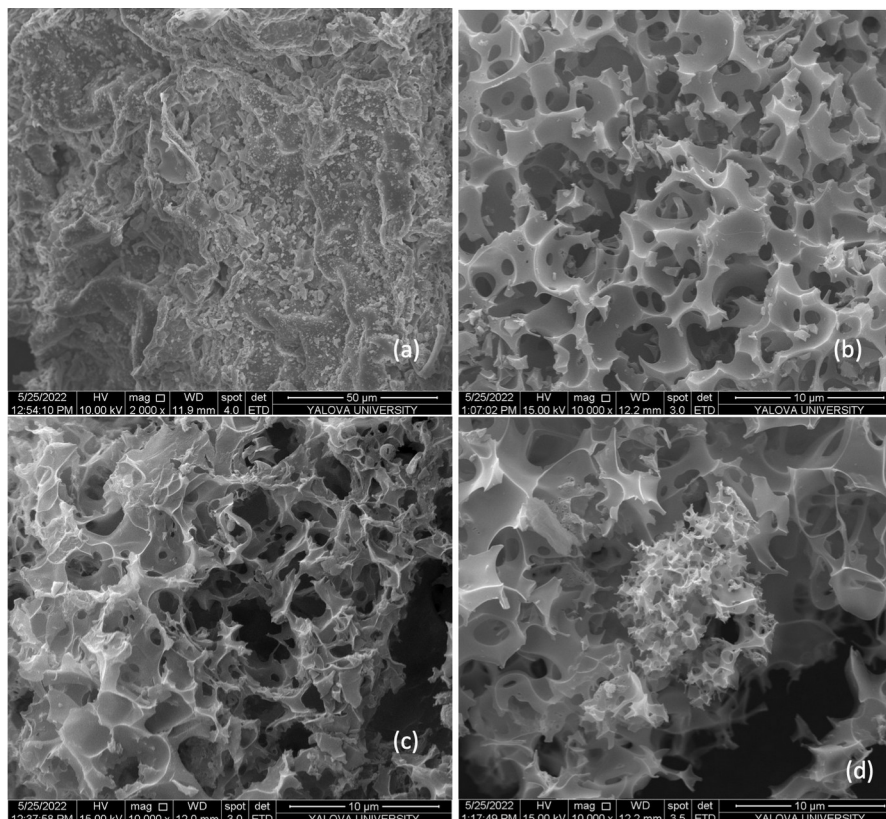


**Figure 7:** SEM images of (a) HTS (magnification of 2000x), (b) ATS, (c) ATP and (d) AHTP (magnification of 10000x).

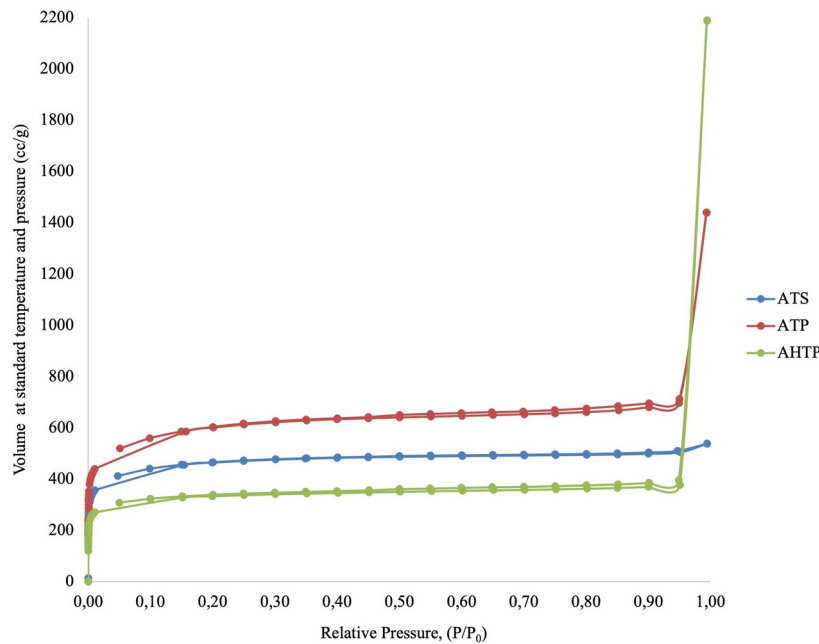
### 3.6. BET Analysis

To have high adsorption capacity, activated carbons should possess morphological properties including amorphous structure, high surface area and high porosity (1). Obtaining  $N_2$  adsorption-desorption isotherms is the most common method used to determine the surface area and pore characteristics of activated carbons. Pores can be classified as micropores (pore diameter <2 nm), mesopores (pore diameter between 2-50 nm), and macropores (pore diameter > 50 nm) (77).

Isothermal plots of ATP, AHTP and ATS are shown in Figure 8.  $N_2$  adsorption-desorption isotherm of ATS is Type I isotherm (based on IUPAC classification), showing microporous characteristics.  $N_2$  isotherm of ATS shows a steep  $N_2$  uptake at very low relative pressures ( $P/P_0 < 0.1$ )

due to  $N_2$ -ATS interactions in narrow micropores by micropore filling (78).

Both ATP and AHTP show Type IV isotherm, with a steep uptake of  $N_2$  at very low relative pressures and a sharp increase of  $N_2$  adsorption at relative pressures higher than 0.9. ATP and AHTP are mesoporous activated carbons. Adsorption of  $N_2$  in mesopores is due to physical interaction between  $N_2$  molecules and activated carbon, and the interaction between  $N_2$  molecules in the condensed state. Since AHTP has larger pores,  $N_2$  adsorption due to condensation is higher. For both AHTP and ATP, hysteresis due to capillary condensation is not observed in the isotherm, showing that mesopores are either smaller in width or in conical/cylindrical form (78).

**Figure 8:** Nitrogen adsorption/desorption isotherms of ATS, ATP and AHTP.

The surface area and pore structure characteristics of ATS, ATP and AHTP are listed in Table 2. ATP has the highest surface area (2056.72  $m^2/g$ ), where 86% of it comes from micropores. This is mainly due to the porosity enhancement by delignification (35, 79) and better accessibility of KOH to the active sites. Similar results were observed in studies that produced activated carbon from cellulose-rich precursors. Tsubota

et al. (21) first delignified bamboo powder with acetic acid-hydrogen peroxide solvent mixture and then carbonized the pulp in the presence of  $CO_2$  at 800 °C. Regardless of the lignin content of the pulp, the surface areas of activated carbons varied between 1062.88  $m^2/g$ -1413  $m^2/g$ , and the average pore sizes varied between 1.7-2 nm.

**Table 2:** Comparison of surface area and pore characteristics.

Sample	$S_{BET}$ ( $m^2/g$ )	$S_{micropore}$ ( $m^2/g$ )	$S_{micropore}/S_{BET}$	Average pore radius (nm)	$V_{micro}$ ( $cm^3/g$ )	$V_{total}$ ( $cm^3/g$ )
ATS	1643	1479.14	0.90	1.01	0.65	0.833
ATP	2056.72	1768.66	0.86	2.16	0.81	2.227
AHTP	1179.71	1055.53	0.89	5.74	0.46	3.386

$S_{BET}$ : Surface area based on multi-point BET analysis

$S_{\text{micropore}}$ : micropore area based on V-t method

$V_{\text{micro}}$ : micropore volume

AHTP, with the largest average pore radius (5.74 nm), has the least micropore volume (0.464 cm<sup>3</sup>/g) and surface area (1179.71 m<sup>2</sup>/g). Sequential hydrothermal pretreatment and organosolv treatment destruct the lignocellulosic structure more resulting in a more porous precursor, which ended with mesoporous structure. ATS, having the lowest average pore radius, is microporous. Activated carbons of different lignocellulosic biomass (which are activated by KOH and carbonized at 800 °C) have similar pore diameter and surface area with ATS (80-84).

### 3.7. Possible Applications of the Microporous and Mesoporous Activated Carbons Prepared from Tea Stalk and Tea Stalk Pulp

This study showed that although the same activation and carbonization conditions are applied, pretreatments namely organosolv delignification and two-step hydrothermal-organosolv treatment affect the pore diameters, surface functional groups and specific surface areas of activated carbons. Nonetheless, those characteristics of activated carbons are important in determining the end use or application. Since the specific surface areas and pore structures of the prepared ATS, ATP and AHTP are different, the most appropriate end-use purpose of those activated carbons should differ. Possible uses are discussed below, considering the specific surface area and pore structure.

One of the processes in which activated carbon is used the most is adsorption. While micropores provide the main adsorption sites, mesopores provide diffusion channels for the adsorbate (85). In liquid and gaseous adsorption processes, the pore size of the adsorbent and the molecular size of the adsorbate must be compatible (85). Due to the reason that gaseous adsorbate molecules are generally found in the range of 0.5–1.5 nm, the microporous activated carbons (average pore size <2 nm) are suitable for the adsorption of gases (86). Microporous activated carbons are mainly used for the adsorption of volatile organic compounds (VOCs), CH<sub>4</sub>, N<sub>2</sub>, and CO<sub>2</sub> (87). Since the presence of oxygen-containing functional groups lowers the adsorption capacity (88, 89), oxygen-rich microporous ATS might not be suitable to be used for the adsorption of VOCs. In the case of CH<sub>4</sub> and N<sub>2</sub> adsorption, it has been shown in studies that the pore size should be quite low (between 0.7 nm and 1.3 nm) for high adsorption capacity (86, 90, 91). Many experimental studies related to CO<sub>2</sub> adsorption show that both the preparation method and structural properties of the activated carbons are similar to ATS. The high specific surface area, micropore structure and presence of highly oxygenated functional groups of ATS make ATS a suitable candidate for CO<sub>2</sub> adsorption. Table 3 shows the structural properties of activated carbons and their CO<sub>2</sub> adsorption capacities that were obtained under similar conditions to our study.

**Table 3:** Structural properties of activated carbons and their CO<sub>2</sub> adsorption capacities reported in similar studies.

Precursor	Carbonization and activation conditions	Surface area (m <sup>2</sup> /g)	Pore size (nm)	Micropore volume (cm <sup>3</sup> /g)	CO <sub>2</sub> adsorption	Ref.
Pine nut shell	KOH/precursor: 2(wt ratio) T: 800 °C	1372	2.1532	0.6842	5.8 mmol/g (0 °C) 3.5 mmol/g (25 °C)	(92)
Walnut shell	KOH/precursor: 1(wt ratio) T: 800 °C	1868	< 4	0.55	9.56 mmol/g (0 °C) 5.17 mmol/g (25 °C) 4.34 mmol/g (40 °C)	(93)
Cucumber peels	KOH/precursor: 1(wt ratio) T: 800 °C	1769	2.334	0.692	6.095 mmol/g (0 °C) 4.37 mmol/g (10 °C) 3.52 mmol/g (25 °C)	(94)
Starch	KOH/precursor: 4 (wt ratio) T: 700 °C	2190	1.2	0.92	5.6 mmol/g (0 °C) 3.5 mmol/g (25 °C) 5.6 mmol/g (50 °C)	(95)
Cellulose	KOH/precursor: 4 (wt ratio) T: 700 °C	2370	1.2	0.96	5.8 mmol/g (0 °C) 3.5 mmol/g (25 °C) 1.8 mmol/g (50 °C)	
Sawdust	KOH/precursor: 4 (wt ratio) T: 700 °C	2250	1.2	0.91	5.5 mmol/g (0 °C) 2.9 mmol/g (25 °C) 1.8 mmol/g (50 °C)	
Sawdust	KOH/precursor: 2 (wt ratio) T: 800 °C	1940	0.9	0.82	5.8 mmol/g (0 °C) 3.9 mmol/g (25 °C) 3.1 mmol/g (50 °C)	(96)
Olive mill waste hydrochar	KOH/precursor: 2 (wt ratio) T: 700 °C	888	< 1	0.294	1.350 mmol/g (0 °C, 1 bar) 2.984 mmol/g (0 °C, 101.3 kPa)	

Camphor leaves	KOH/precursor: 2 (wt ratio) T: 800 °C	1736	< 1	0.357	4.8 mmol/g (0 °C) 2.42 mmol/g (25 °C) 1.45 mmol/g (50 °C)	(97)
Pristine wheat flour	KOH/precursor: 2 (wt ratio) T: 700 °C	1057	< 2	0.474	4.41 mmol/g (0 °C) 2.77 mmol/g (25 °C) 1.60 mmol/g (50 °C)	(98)
Peanut shell	KOH/precursor: 1 (wt ratio) T: 700 °C	956	<11	Not available	1.54 mmol/g (25 °C, 0.15 bar)	(99)
Sunflower seed shell	KOH/precursor: 1.25 (wt ratio) T: 700 °C	1790	< 1	Not available	1.46 mmol/g (25 °C, 0.15 bar)	
Pine nut shell	KOH/precursor: 2 (wt ratio) T: 700 °C	Not available	<1.1	Not available	7.7 mmol/g (0 °C, 1 bar) 5 mmol/g (25 °C, 1 bar) 3.3 mmol/g (0 °C, 0.15 bar) 2 mmol/g (25 °C, 0.15 bar)	(100)
Paulownia sawdust	KOH/precursor: 2 (wt ratio) T: 700 °C	831	<1	0.297	6.83 mmol/g (0 °C)	(101)
Paulownia sawdust	KOH/precursor: 4 (wt ratio) T: 800 °C	1555	<1	0.598	7.14 mmol/g (0 °C)	
Spent coffee grounds	KOH/precursor: 3 (wt ratio) T: 700 °C	1082	3	0.44	3.2 mmol/g (0 °C, 101 kPa) 2.7 mmol/g (25°C, 101 kPa)	(102)

Mesoporous activated carbons (2 nm < average pore size <50 nm) are more preferred in the adsorption of large molecules including dyes, pharmaceuticals,

cyanobacterial toxins, pollutants and enzymes (103-105).

**Table 4:** Structural properties of mesoporous activated carbons and their reported adsorbates and adsorption capacities reported in similar studies.

Precursor	Carbonization and activation conditions	Surface area (m <sup>2</sup> /g)	Pore size (nm)	Micropore volume (cm <sup>3</sup> /g)	Adsorbate and adsorption capacity	Ref.
Dragon fruit peels	KOH/precursor: 2 (wt ratio) T: 700 °C	756.3	11.3	0.376	Adsorbate: methylene blue dye Maximum adsorption capacity: 195.2 mg/g	(106)
Yellow mombin fruit stones	KOH/precursor: 1 (wt ratio) T: 500 °C	167	4.82	0.027	Adsorbate: Dianix ® royal blue dye Maximum adsorption capacity: 82.28 mg/g	(107)
Rice straw	Precursor was soaked in 85 wt % KOH solution T: 400 °C for 1 h and then 700 °C for 1 h.	165.9	5.941	0.032	Adsorbate: Methylene blue dye Maximum adsorption capacity: 392.4 mg/g Adsorbate: Congo red dye Maximum adsorption capacity: 178.4 mg/g	(108)
Rice straw	Precursor was first pre-carbonized at 400 °C for 1 h, then soaked in 85 wt% KOH solution, then carbonized at 700 °C for 1 h.	1973	2.292	0.769	Adsorbate: Methylene blue dye Maximum adsorption capacity: 527.6 mg/g Adsorbate: Congo red dye Maximum adsorption capacity: 531.4 mg/g	(109)
Sugarcane bagasse	KOH/precursor: 1 (wt ratio) T: 700 °C	1204	1.79	0.57	Adsorbate: Phenol Maximum adsorption capacity: 88 mg/g	(109)
Sawdust	KOH/precursor: 1 (wt ratio) T: 700 °C	1544	1.82	0.69	Adsorbate: Phenol Maximum adsorption capacity: 96.8 mg/g	(109)
Potato peel	KOH/precursor: 4 (wt ratio) T: 600 °C	2394	<10 Average between: 2-4 nm	-	Adsorbate: Methylene Blue Maximum adsorption capacity: 2521 mg/g	(110)
Crab shell	KOH/precursor: 3 (wt ratio) T: 800 °C	1095.14	2.18	-	Adsorbate: Tetracycline Maximum adsorption capacity: 380.92 mg/g	(111)

Mesoporous activated carbons are also preferred as electrode materials in supercapacitors due to their high specific surface area, high pore volume, good thermal stability, and enhanced specific capacitance (112, 113). Apart from mesoporous structure, presence of oxygen-containing functional groups on the surface of the activated carbon also enhances electrochemical active sites (111). Table 5 shows the studies in which activated carbon was prepared under conditions similar to those

we applied in the present study and used in supercapacitors. According to the studies in Table 5, having pores with a diameter of 2-5 nm enhances the transport of electrolytes. The large specific surface area, the presence of macropores alongside micropores, and the abundance of oxygenated functional groups make ATP and AHTP a suitable candidate for use in supercapacitors.

**Table 5:** Structural properties of activated carbons and their maximum specific capacitance reported in similar studies.

Precursor	Carbonization and activation conditions	Surface area (m <sup>2</sup> /g)	Pore size (nm)	Pore volume (cm <sup>3</sup> /g)	Maximum specific capacitance (F/g)	Ref.
Corncob	Carbonization at 400 °C for 4 h, then activation with KOH (KOH/precursor: 3 (wt ratio) ) at 600 °C	800	Micropores in the range of 1.4-1.8 nm, mesopores in the range of 2.2-5 nm	0.337	390	(114)
Wastewater from vitamin C production, template: melamine foam	KOH/precursor: 5 (wt ratio) T: 700 °C	3837	2.32	2.22	217	(113)
Olive tree branches	Carbonization: 500 °C for 2 h Activation: KOH/precursor: 4 (wt ratio) 800 °C for 82 min	2980	0.8nm<pore size<5 nm	1.59	410	(115)
Biogas slurry	First drying, then carbonization at 650 °C for 1 h. Activation: KOH/precursor: 3 (wt ratio) 700 °C for 30 min	326.7	4.7	0.24	163	(116)
	First drying, then carbonization at 650 °C for 1 h. Activation: KOH/precursor: 3 (wt ratio) 700 °C for 60 min	514.7	4.7	0.38	182	
Coconut silk	Carbonization at 400 °C for 1 h. Activation: KOH/precursor: 4 (wt ratio) 900 °C for 1 h	2318	0.5- 5 (average 1.42)	0.87	631	(111)
Corn silk	Carbonization at 300 °C for 2 h. Activation: KOH/precursor: 3 (wt ratio) 850 °C for 4 h	2441	3.097 (average) (large pores (>30nm) were also seen in the structure)	1.890	174	(117)

#### 4. CONCLUSION

In the present study, three different activated carbons were prepared: activated carbon from tea stalk itself, activated carbon from tea stalk pulp obtained by using glycerol organosolv pretreatment, and activated carbon from tea stalk hydrochar pulp obtained by using sequential hydrothermal pretreatment-organosolv delignification. The tea stalk itself and the cellulose-rich precursors were carbonized at 800 °C for 1 h in the presence of KOH.

The study showed that partial removal of lignin yielded activated carbons with more specific surface area and mesopores. Additionally, because delignification modified the functional groups of the biomass, the surface of activated carbon contained more oxygen-rich functional groups. While decreasing the lignin removal, hydrothermal pretreatment prior to delignification

ended up with mesoporous activated carbon with a larger pore diameter. Activated carbons (ATS, ATP and AHTP) obtained from tea stalk can be used in many applications from environmental applications to energy storage due to their different surface areas, micropore volumes and pore structures.

#### 5. CONFLICT OF INTEREST

The authors declare that they have no known competing financial interests or personal relationships that could have appeared to influence the work reported in this paper.

## 6. ACKNOWLEDGMENTS

This research was financially supported by Yalova University Scientific Research Unit [Project No: 2020/AP/0007].

## 7. REFERENCES

1. Adeleye AT, Akande AA, Odoh CK, Philip M, Fidelis TT, Amos PI, et al. Efficient synthesis of bio-based activated carbon (AC) for catalytic systems: A green and sustainable approach. *J Ind Eng Chem* [Internet]. 2021 Apr 25;96:59–75. Available from: [<URL>](#).
2. Darmawan S, Wistara NJ, Pari G, Maddu A, Syafii W. Characterization of Lignocellulosic Biomass as Raw Material for the Production of Porous Carbon-based Materials. *BioResources* [Internet]. 2016 Feb 29;11(2):3561–74. Available from: [<URL>](#).
3. De Bhowmick G, Sarmah AK, Sen R. Lignocellulosic biorefinery as a model for sustainable development of biofuels and value added products. *Bioresour Technol* [Internet]. 2018 Jan 1;247:1144–54. Available from: [<URL>](#).
4. Astuti W, Sulistyarningsih T, Prastiyanto D, Rusiyanto, Lanjar, Riayanti FI, et al. Influence of lignocellulosic composition in biomass waste on the microstructure and dye adsorption characteristics of microwave-assisted ZnCl<sub>2</sub> activated carbon. *Biomass Convers Biorefinery* [Internet]. 2023 May 10;1:1–17. Available from: [<URL>](#).
5. Nabais JMV, Gomes JA, Suhas, Carrott PJM, Laginhas C, Roman S. Phenol removal onto novel activated carbons made from lignocellulosic precursors: Influence of surface properties. *J Hazard Mater* [Internet]. 2009 Aug 15;167(1–3):904–10. Available from: [<URL>](#).
6. Chen S, Xia Y, Zhang B, Chen H, Chen G, Tang S. Disassembly of lignocellulose into cellulose, hemicellulose, and lignin for preparation of porous carbon materials with enhanced performances. *J Hazard Mater* [Internet]. 2021 Apr 15;408:124956. Available from: [<URL>](#).
7. Chanpee S, Kaewtrakulchai N, Khemasiri N, Eiad-ua A, Assawaengrat P. Nanoporous Carbon from Oil Palm Leaves via Hydrothermal Carbonization-Combined KOH Activation for Paraquat Removal. *Molecules* [Internet]. 2022 Aug 19;27(16):5309. Available from: [<URL>](#).
8. Demiral H, Demiral İ, Tümsek F, Karabacakoğlu B. Adsorption of chromium(VI) from aqueous solution by activated carbon derived from olive bagasse and applicability of different adsorption models. *Chem Eng J* [Internet]. 2008 Oct 15;144(2):188–96. Available from: [<URL>](#).
9. Olivares-Marín M, Fernández JA, Lázaro MJ, Fernández-González C, Macías-García A, Gómez-Serrano V, et al. Cherry stones as precursor of activated carbons for supercapacitors. *Mater Chem Phys* [Internet]. 2009 Mar 15;114(1):323–7. Available from: [<URL>](#).
10. Martínez de Yuso A, Izquierdo MT, Valenciano R, Rubio B. Toluene and n-hexane adsorption and recovery behavior on activated carbons derived from almond shell wastes. *Fuel Process Technol* [Internet]. 2013 Jun 1;110:1–7. Available from: [<URL>](#).
11. Mohamad Nor N, Lau LC, Lee KT, Mohamed AR. Synthesis of activated carbon from lignocellulosic biomass and its applications in air pollution control—a review. *J Environ Chem Eng* [Internet]. 2013 Dec 1;1(4):658–66. Available from: [<URL>](#).
12. González-García P. Activated carbon from lignocellulosics precursors: A review of the synthesis methods, characterization techniques and applications. *Renew Sustain Energy Rev* [Internet]. 2018 Feb 1;82:1393–414. Available from: [<URL>](#).
13. Mohd Azmi NZ, Buthiyappan A, Abdul Raman AA, Abdul Patah MF, Sufian S. Recent advances in biomass based activated carbon for carbon dioxide capture – A review. *J Ind Eng Chem* [Internet]. 2022 Dec 25;116:1–20. Available from: [<URL>](#).
14. Khezami L, Chetouani A, Taouk B, Capart R. Production and characterisation of activated carbon from wood components in powder: Cellulose, lignin, xylan. *Powder Technol* [Internet]. 2005 Sep 29;157(1–3):48–56. Available from: [<URL>](#).
15. Suhas, Carrott PJM, Ribeiro Carrott MML. Lignin – from natural adsorbent to activated carbon: A review. *Bioresour Technol* [Internet]. 2007 Sep 1;98(12):2301–12. Available from: [<URL>](#).
16. Xi Y, Yang D, Qiu X, Wang H, Huang J, Li Q. Renewable lignin-based carbon with a remarkable electrochemical performance from potassium compound activation. *Ind Crops Prod* [Internet]. 2018 Nov 15;124:747–54. Available from: [<URL>](#).
17. Gayathiri M, Pulingam T, Lee KT, Sudesh K. Activated carbon from biomass waste precursors: Factors affecting production and adsorption mechanism. *Chemosphere* [Internet]. 2022 May 1;294:133764. Available from: [<URL>](#).
18. Guo Y, Rockstraw DA. Physical and chemical properties of carbons synthesized from xylan, cellulose, and Kraft lignin by H<sub>3</sub>PO<sub>4</sub> activation. *Carbon N Y* [Internet]. 2006 Jul 1;44(8):1464–75. Available from: [<URL>](#).
19. Cagnon B, Py X, Guillot A, Stoeckli F, Chambat G. Contributions of hemicellulose, cellulose and lignin to the mass and the porous properties of chars and steam activated carbons from various lignocellulosic precursors. *Bioresour Technol* [Internet]. 2009 Jan

- 1;100(1):292–8. Available from: [<URL>](#).
20. Rodriguez Correa C, Otto T, Kruse A. Influence of the biomass components on the pore formation of activated carbon. *Biomass and Bioenergy* [Internet]. 2017 Feb 1;97:53–64. Available from: [<URL>](#).
21. Tsubota T, Nagata D, Kamimura S, Ohno T. Partial Delignification as Pretreatment for Nanoporous Carbon Material from Biomass. *J Nanosci Nanotechnol* [Internet]. 2017 Jan 1;17(1):815–20. Available from: [<URL>](#).
22. Gao Y, Aliques Tomas M del C, Garemark J, Sheng X, Berglund L, Li Y. Olive Stone Delignification Toward Efficient Adsorption of Metal Ions. *Front Mater* [Internet]. 2021 Feb 12;8:605931. Available from: [<URL>](#).
23. Keplinger T, Wittel FK, Rüggeberg M, Burgert I. Wood Derived Cellulose Scaffolds—Processing and Mechanics. *Adv Mater* [Internet]. 2021 Jul 14;33(28):2001375. Available from: [<URL>](#).
24. Mittal N, Kaur M, Singh V. Adsorption studies on hydrophobic disperse dye using cellulose derived mesoporous activated carbon. In: 9th International Conference on Advancements and Futuristic Trends in Mechanical and Materials Engineering (AFTMME) [Internet]. Rupnagar; 2021. Available from: [<URL>](#).
25. Han S, Wang J, Wang L. Preparation of hydrophobic, porous, and flame-resistant lignocellulosic carbon material by pyrolyzing delignified wood. *Vacuum* [Internet]. 2022 Mar 1;197:110867. Available from: [<URL>](#).
26. Sun M, Hong L. Impacts of the pendant functional groups of cellulose precursor on the generation of pore structures of activated carbons. *Carbon N Y* [Internet]. 2011 Jun 1;49(7):2173–80. Available from: [<URL>](#).
27. Banu Jamaldeen S, Kurade MB, Basak B, Yoo CG, Oh KK, Jeon B-H, et al. A review on physico-chemical delignification as a pretreatment of lignocellulosic biomass for enhanced bioconversion. *Bioresour Technol* [Internet]. 2022 Feb 1;346:126591. Available from: [<URL>](#).
28. Sun C, Song G, Pan Z, Tu M, Kharaziha M, Zhang X, et al. Advances in organosolv modified components occurring during the organosolv pretreatment of lignocellulosic biomass. *Bioresour Technol* [Internet]. 2023 Jan 1;368:128356. Available from: [<URL>](#).
29. Zhang Z, Harrison MD, Rackemann DW, Doherty WOS, O'Hara IM. Organosolv pretreatment of plant biomass for enhanced enzymatic saccharification. *Green Chem* [Internet]. 2016 Jan 18;18(2):360–81. Available from: [<URL>](#).
30. Ferreira JA, Taherzadeh MJ. Improving the economy of lignocellulose-based biorefineries with organosolv pretreatment. *Bioresour Technol* [Internet]. 2020 Mar 1;299:122695. Available from: [<URL>](#).
31. Vargas F, Domínguez E, Vila C, Rodríguez A, Garrote G. Biorefinery Scheme for Residual Biomass Using Autohydrolysis and Organosolv Stages for Oligomers and Bioethanol Production. *Energy & Fuels* [Internet]. 2016 Oct 20;30(10):8236–45. Available from: [<URL>](#).
32. Espirito Santo M, Rezende CA, Bernardinelli OD, Pereira N, Curvelo AAS, deAzevedo ER, et al. Structural and compositional changes in sugarcane bagasse subjected to hydrothermal and organosolv pretreatments and their impacts on enzymatic hydrolysis. *Ind Crops Prod* [Internet]. 2018 Mar 1;113:64–74. Available from: [<URL>](#).
33. Ibrahim Q, Kruse A. Prehydrolysis and organosolv delignification process for the recovery of hemicellulose and lignin from beech wood. *Bioresour Technol Reports* [Internet]. 2020 Sep 1;11:100506. Available from: [<URL>](#).
34. Vedoya CI, Vallejos ME, Area MC, Felissia FE, Raffaeli N, da Silva Curvelo AA. Hydrothermal treatment and organosolv pulping of softwood assisted by carbon dioxide. *Ind Crops Prod* [Internet]. 2020 May 1;147:112244. Available from: [<URL>](#).
35. Guo K-N, Zhang C, Xu L-H, Sun S-C, Wen J-L, Yuan T-Q. Efficient fractionation of bamboo residue by autohydrolysis and deep eutectic solvents pretreatment. *Bioresour Technol* [Internet]. 2022 Jun 1;354:127225. Available from: [<URL>](#).
36. Sun Q, Chen W-J, Pang B, Sun Z, Lam SS, Sonne C, et al. Ultrastructural change in lignocellulosic biomass during hydrothermal pretreatment. *Bioresour Technol* [Internet]. 2021 Dec 1;341:125807. Available from: [<URL>](#).
37. Sun D, Lv Z-W, Rao J, Tian R, Sun S-N, Peng F. Effects of hydrothermal pretreatment on the dissolution and structural evolution of hemicelluloses and lignin: A review. *Carbohydr Polym* [Internet]. 2022 Apr 1;281:119050. Available from: [<URL>](#).
38. Scapini T, dos Santos MSN, Bonatto C, Wancura JHC, Mulinari J, Camargo AF, et al. Hydrothermal pretreatment of lignocellulosic biomass for hemicellulose recovery. *Bioresour Technol* [Internet]. 2021 Dec 1;342:126033. Available from: [<URL>](#).
39. Cavali M, Libardi Junior N, de Sena JD, Woiciechowski AL, Soccol CR, Belli Filho P, et al. A review on hydrothermal carbonization of potential biomass wastes, characterization and environmental applications of hydrochar, and biorefinery perspectives of the process. *Sci Total Environ* [Internet]. 2023 Jan 20;857:159627. Available from: [<URL>](#).
40. Lachos-Perez D, César Torres-Mayanga P, Abaide ER, Zabot GL, De Castilhos F. Hydrothermal carbonization and Liquefaction: differences, progress, challenges, and

- opportunities. *Bioresour Technol* [Internet]. 2022 Jan 1;343:126084. Available from: [<URL>](#).
41. Başakçılardan Kabakcı S, Baran SS. Hydrothermal carbonization of various lignocellulosics: Fuel characteristics of hydrochars and surface characteristics of activated hydrochars. *Waste Manag* [Internet]. 2019 Dec 1;100:259–68. Available from: [<URL>](#).
42. Başakçılardan Kabakcı S, Tanış MH. Pretreatment of lignocellulosic biomass at atmospheric conditions by using different organosolv liquors: a comparison of lignins. *Biomass Convers Biorefinery* [Internet]. 2021 Dec 21;11(6):2869–80. Available from: [<URL>](#).
43. García R, Pizarro C, Lavín AG, Bueno JL. Biomass proximate analysis using thermogravimetry. *Bioresour Technol* [Internet]. 2013 Jul 1;139:1–4. Available from: [<URL>](#).
44. Sluiter A, Hames B, Ruiz R, Scarlata C, Sluiter J, Templeton D, et al. Determination of Structural Carbohydrates and Lignin in Biomass Laboratory Analytical Procedure (LAP) Issue Date: 7/17/2005. 2008; Available from: [<URL>](#).
45. Md Salim R, Asik J, Sarjadi MS. Chemical functional groups of extractives, cellulose and lignin extracted from native *Leucaena leucocephala* bark. *Wood Sci Technol* [Internet]. 2021 Mar 23;55(2):295–313. Available from: [<URL>](#).
46. Güleç F, Riesco LMG, Williams O, Kostas ET, Samson A, Lester E. Hydrothermal conversion of different lignocellulosic biomass feedstocks – Effect of the process conditions on hydrochar structures. *Fuel* [Internet]. 2021 Oct 15;302:121166. Available from: [<URL>](#).
47. Fan Y, Cai Y, Li X, Jiao L, Xia J, Deng X. Effects of the cellulose, xylan and lignin constituents on biomass pyrolysis characteristics and bio-oil composition using the Simplex Lattice Mixture Design method. *Energy Convers Manag* [Internet]. 2017 Apr 15;138:106–18. Available from: [<URL>](#).
48. de Moraes Teixeira E, Corrêa AC, Manzoli A, de Lima Leite F, de Oliveira CR, Mattoso LHC. Cellulose nanofibers from white and naturally colored cotton fibers. *Cellulose* [Internet]. 2010 Jun 12;17(3):595–606. Available from: [<URL>](#).
49. Kim DY, Nishiyama Y, Wada M, Kuga S. High-yield carbonization of cellulose by sulfuric acid impregnation. *Cellulose* [Internet]. 2001;8(1):29–33. Available from: [<URL>](#).
50. Guo F, He Y, Hassanpour A, Gardy J, Zhong Z. Thermogravimetric analysis on the co-combustion of biomass pellets with lignite and bituminous coal. *Energy* [Internet]. 2020 Apr 15;197:117147. Available from: [<URL>](#).
51. Kwasi Opoku B, Isaac A, Akrofi Micheal A, Kwesi Bentum J, Paul Muyoma W. Characterization of Chemically Activated Carbons Produced from Coconut and Palm Kernel Shells Using SEM and FTIR Analyses. *Am J Appl Chem* [Internet]. 2021;9(3):90–6. Available from: [<URL>](#).
52. Zhang Z, Xu L, Liu Y, Feng R, Zou T, Zhang Y, et al. Efficient removal of methylene blue using the mesoporous activated carbon obtained from mangosteen peel wastes: Kinetic, equilibrium, and thermodynamic studies. *Microporous Mesoporous Mater* [Internet]. 2021 Feb 1;315:110904. Available from: [<URL>](#).
53. Abbasi S, Hekmat F, Shahrokhian S. Dual redox electrolytes for improving the performance of asymmetric supercapacitors constructed from heteroatom-doped green carbon spheres. *J Alloys Compd* [Internet]. 2023 Sep 25;957:170452. Available from: [<URL>](#).
54. Zhou H, Fu H, Wu X, Wu B, Dai C. Discrimination of tea varieties based on FTIR spectroscopy and an adaptive improved possibilistic c-means clustering. *J Food Process Preserv* [Internet]. 2020 Oct 1;44(10):e14795. Available from: [<URL>](#).
55. Yu S, Xie M, Li Q, Zhang Y, Zhou H. Evolution of kraft lignin during hydrothermal treatment under different reaction conditions. *J Energy Inst* [Internet]. 2022 Aug 1;103:147–53. Available from: [<URL>](#).
56. Wan C, Jiao Y, Wei S, Li X, Tian W, Wu Y, et al. Scalable Top-to-Bottom Design on Low Tortuosity of Anisotropic Carbon Aerogels for Fast and Reusable Passive Capillary Absorption and Separation of Organic Leakages. *ACS Appl Mater Interfaces* [Internet]. 2019 Dec 26;11(51):47846–57. Available from: [<URL>](#).
57. Ferrer A, Alciaturi C, Faneite A, Ríos J. Analyses of Biomass Fibers by XRD, FT-IR, and NIR. In: *Analytical Techniques and Methods for Biomass* [Internet]. Cham: Springer International Publishing; 2016. p. 45–83. Available from: [<URL>](#).
58. Pezoti O, Cazetta AL, Bedin KC, Souza LS, Martins AC, Silva TL, et al. NaOH-activated carbon of high surface area produced from guava seeds as a high-efficiency adsorbent for amoxicillin removal: Kinetic, isotherm and thermodynamic studies. *Chem Eng J* [Internet]. 2016 Mar 15;288:778–88. Available from: [<URL>](#).
59. Ali R, Aslam Z, Shawabkeh RA, Asghar A, Hussein IA. BET, FTIR, and RAMAN characterizations of activated carbon from wasteoil fly ash. *TURKISH J Chem* [Internet]. 2020 Apr 1;44(2):279–95. Available from: [<URL>](#).
60. Haghbin MR, Niknam Shahrak M. Process conditions optimization for the fabrication of highly porous activated carbon from date palm bark wastes for

- removing pollutants from water. Powder Technol [Internet]. 2021 Jan 2;377:890–9. Available from: [<URL>](#).
61. Njoku VO, Islam MA, Asif M, Hameed BH. Adsorption of 2,4-dichlorophenoxyacetic acid by mesoporous activated carbon prepared from H<sub>3</sub>PO<sub>4</sub>-activated langsat empty fruit bunch. J Environ Manage [Internet]. 2015 May 1;154:138–44. Available from: [<URL>](#).
62. Islam MS, Ang BC, Gharekhani S, Afifi ABM. Adsorption capability of activated carbon synthesized from coconut shell. Carbon Lett [Internet]. 2016 Oct 31;20:1–9. Available from: [<URL>](#).
63. Zhang J, Yu L, Wang Z, Tian Y, Qu Y, Wang Y, et al. Spherical microporous/mesoporous activated carbon from pulping black liquor. J Chem Technol Biotechnol [Internet]. 2011 Sep 1;86(9):1177–83. Available from: [<URL>](#).
64. Li J, Li K, Zhang T, Wang S, Jiang Y, Bao Y, et al. Development of Activated carbon from Windmill palm sheath fiber by KOH activation. Fibers Polym [Internet]. 2016 Jun 6;17(6):880–7. Available from: [<URL>](#).
65. Chakraborty I, Rongpipi S, Govindaraju I, B R, Mal SS, Gomez EW, et al. An insight into microscopy and analytical techniques for morphological, structural, chemical, and thermal characterization of cellulose. Microsc Res Tech [Internet]. 2022 May 18;85(5):1990–2015. Available from: [<URL>](#).
66. Barbash VA, Yaschenko O V., Shniruk OM. Preparation and Properties of Nanocellulose from Organosolv Straw Pulp. Nanoscale Res Lett [Internet]. 2017 Dec 31;12(1):241. Available from: [<URL>](#).
67. Buendia-Kandia F, Brosse N, Petitjean D, Mauviel G, Rondags E, Guedon E, et al. Hydrothermal conversion of wood, organosolv, and chlorite pulps. Biomass Convers Biorefinery [Internet]. 2020 Mar 7;10(1):1–13. Available from: [<URL>](#).
68. Tang S, Liu R, Sun FF, Dong C, Wang R, Gao Z, et al. Bioprocessing of tea oil fruit hull with acetic acid organosolv pretreatment in combination with alkaline H<sub>2</sub>O<sub>2</sub>. Biotechnol Biofuels [Internet]. 2017 Dec 8;10(1):86. Available from: [<URL>](#).
69. Song X, Jiang Y, Rong X, Wei W, Wang S, Nie S. Surface characterization and chemical analysis of bamboo substrates pretreated by alkali hydrogen peroxide. Bioresour Technol [Internet]. 2016 Sep 1;216:1098–101. Available from: [<URL>](#).
70. Zhang J, Wang Y, Zhang L, Zhang R, Liu G, Cheng G. Understanding changes in cellulose crystalline structure of lignocellulosic biomass during ionic liquid pretreatment by XRD. Bioresour Technol [Internet]. 2014 Jan 1;151:402–5. Available from: [<URL>](#).
71. Fan J, Li F, Fang D, Chen Q, Chen Q, Wang H, et al. Effects of hydrophobic coating on properties of hydrochar produced at different temperatures: Specific surface area and oxygen-containing functional groups. Bioresour Technol [Internet]. 2022 Nov 1;363:127971. Available from: [<URL>](#).
72. Sun FF, Wang L, Hong J, Ren J, Du F, Hu J, et al. The impact of glycerol organosolv pretreatment on the chemistry and enzymatic hydrolyzability of wheat straw. Bioresour Technol [Internet]. 2015 Jul 1;187:354–61. Available from: [<URL>](#).
73. Dong H, Zhang L, Shao L, Wu Z, Zhan P, Zhou X, et al. Versatile Strategy for the Preparation of Woody Biochar with Oxygen-Rich Groups and Enhanced Porosity for Highly Efficient Cr(VI) Removal. ACS Omega [Internet]. 2022 Jan 11;7(1):863–74. Available from: [<URL>](#).
74. Szewczyk I, Kosydar R, Natkański P, Duraczyńska D, Gurgul J, Kuśtrowski P, et al. Effect of the type of siliceous template and carbon precursor on physicochemical and catalytic properties of mesoporous nanostructured carbon-palladium systems. J Porous Mater [Internet]. 2020 Oct 24;27(5):1287–308. Available from: [<URL>](#).
75. Cheng C, He Q, Ismail TM, Mosqueda A, Ding L, Yu J, et al. Hydrothermal carbonization of rape straw: Effect of reaction parameters on hydrochar and migration of AAEMs. Chemosphere [Internet]. 2022 Mar 1;291:132785. Available from: [<URL>](#).
76. Wang S, Zhao S, Cheng X, Qian L, Barati B, Gong X, et al. Study on two-step hydrothermal liquefaction of macroalgae for improving bio-oil. Bioresour Technol [Internet]. 2021 Jan 1;319:124176. Available from: [<URL>](#).
77. Chatterjee S, Saito T. Lignin-Derived Advanced Carbon Materials. ChemSusChem [Internet]. 2015 Dec 16;8(23):3941–58. Available from: [<URL>](#).
78. Thommes M, Kaneko K, Neimark A V., Olivier JP, Rodriguez-Reinoso F, Rouquerol J, et al. Physisorption of gases, with special reference to the evaluation of surface area and pore size distribution (IUPAC Technical Report). Pure Appl Chem [Internet]. 2015 Oct 1;87(9–10):1051–69. Available from: [<URL>](#).
79. Zheng K, Xiao L. Iron and nitrogen co-doped porous carbon derived from natural cellulose of wood activating peroxydisulfate for degradation of tetracycline: Role of delignification and mechanisms. Int J Biol Macromol [Internet]. 2022 Dec 1;222:2041–53. Available from: [<URL>](#).
80. Mistar EM, Alfatah T, Supardan MD. Synthesis and characterization of activated carbon from Bambusa vulgaris striata using two-step KOH activation. J Mater Res Technol [Internet]. 2020 May 1;9(3):6278–86. Available from: [<URL>](#).

81. Guo Y, Wang Q. Fabrication and Characterization of Activated Carbon from *Phyllostachys edulis* Using Single-Step KOH Activation with Different Temperatures. *Processes* [Internet]. 2022 Aug 28;10(9):1712. Available from: [<URL>](#).
82. Zhang H, Xing L, Liang H, Ren J, Ding W, Wang Q, et al. Efficient removal of Remazol Brilliant Blue R from water by a cellulose-based activated carbon. *Int J Biol Macromol* [Internet]. 2022 May 15;207:254–62. Available from: [<URL>](#).
83. Thongpat W, Taweekun J, Maliwan K. Synthesis and characterization of microporous activated carbon from rubberwood by chemical activation with KOH. *Carbon Lett* [Internet]. 2021 Oct 22;31(5):1079–88. Available from: [<URL>](#).
84. Abuelnoor N, AlHajaj A, Khaleel M, Vega LF, Abu-Zahra MRM. Activated carbons from biomass-based sources for CO<sub>2</sub> capture applications. *Chemosphere* [Internet]. 2021 Nov 1;282:131111. Available from: [<URL>](#).
85. Wang X, Cheng H, Ye G, Fan J, Yao F, Wang Y, et al. Key factors and primary modification methods of activated carbon and their application in adsorption of carbon-based gases: A review. *Chemosphere* [Internet]. 2022 Jan 1;287:131995. Available from: [<URL>](#).
86. Blanco AAG, de Oliveira JCA, López R, Moreno-Piraján JC, Giraldo L, Zgrablich G, et al. A study of the pore size distribution for activated carbon monoliths and their relationship with the storage of methane and hydrogen. *Colloids Surfaces A Physicochem Eng Asp* [Internet]. 2010 Mar 20;357(1–3):74–83. Available from: [<URL>](#).
87. Wang Q, Yu Y, Li Y, Min X, Zhang J, Sun T. Methane separation and capture from nitrogen rich gases by selective adsorption in microporous Materials: A review. *Sep Purif Technol* [Internet]. 2022 Jan 15;283:120206. Available from: [<URL>](#).
88. Lillo-Ródenas MA, Cazorla-Amorós D, Linares-Solano A. Behaviour of activated carbons with different pore size distributions and surface oxygen groups for benzene and toluene adsorption at low concentrations. *Carbon N Y* [Internet]. 2005 Jul 1;43(8):1758–67. Available from: [<URL>](#).
89. Zhu R, Yu Q, Li M, Zhao H, Jin S, Huang Y, et al. Analysis of factors influencing pore structure development of agricultural and forestry waste-derived activated carbon for adsorption application in gas and liquid phases: A review. *J Environ Chem Eng* [Internet]. 2021 Oct 1;9(5):105905. Available from: [<URL>](#).
90. Liu C, Dang Y, Zhou Y, Liu J, Sun Y, Su W, et al. Effect of carbon pore structure on the CH<sub>4</sub>/N<sub>2</sub> separation. *Adsorption* [Internet]. 2012 Nov 5;18(3–4):321–5. Available from: [<URL>](#).
91. Djeridi W, Ouederni A, Wiersum AD, Llewellyn PL, El Mir L. High pressure methane adsorption on microporous carbon monoliths prepared by olives stones. *Mater Lett* [Internet]. 2013 May 15;99:184–7. Available from: [<URL>](#).
92. Tang Z, Gao J, Zhang Y, Du Q, Feng D, Dong H, et al. Ultra-microporous biochar-based carbon adsorbents by a facile chemical activation strategy for high-performance CO<sub>2</sub> adsorption. *Fuel Process Technol* [Internet]. 2023 Mar 1;241:107613. Available from: [<URL>](#).
93. Serafin J, Dziejarski B, Cruz Junior OF, Sreńscek-Nazzal J. Design of highly microporous activated carbons based on walnut shell biomass for H<sub>2</sub> and CO<sub>2</sub> storage. *Carbon N Y* [Internet]. 2023 Jan 5;201:633–47. Available from: [<URL>](#).
94. Kamran U, Rhee KY, Lee S-Y, Park S-J. Solvent-free conversion of cucumber peels to N-doped microporous carbons for efficient CO<sub>2</sub> capture performance. *J Clean Prod* [Internet]. 2022 Oct 1;369:133367. Available from: [<URL>](#).
95. Sevilla M, Fuertes AB. Sustainable porous carbons with a superior performance for CO<sub>2</sub> capture. *Energy Environ Sci* [Internet]. 2011 Apr 28;4(5):1765–71. Available from: [<URL>](#).
96. González B, Manyà JJ. Activated olive mill waste-based hydrochars as selective adsorbents for CO<sub>2</sub> capture under postcombustion conditions. *Chem Eng Process - Process Intensif* [Internet]. 2020 Mar 1;149:107830. Available from: [<URL>](#).
97. Xu J, Shi J, Cui H, Yan N, Liu Y. Preparation of nitrogen doped carbon from tree leaves as efficient CO<sub>2</sub> adsorbent. *Chem Phys Lett* [Internet]. 2018 Nov 1;711:107–12. Available from: [<URL>](#).
98. Hong S-M, Jang E, Dysart AD, Pol VG, Lee KB. CO<sub>2</sub> Capture in the Sustainable Wheat-Derived Activated Microporous Carbon Compartments. *Sci Rep* [Internet]. 2016 Oct 4;6(1):34590. Available from: [<URL>](#).
99. Deng S, Hu B, Chen T, Wang B, Huang J, Wang Y, et al. Activated carbons prepared from peanut shell and sunflower seed shell for high CO<sub>2</sub> adsorption. *Adsorption* [Internet]. 2015 Feb 23;21(1–2):125–33. Available from: [<URL>](#).
100. Deng S, Wei H, Chen T, Wang B, Huang J, Yu G. Superior CO<sub>2</sub> adsorption on pine nut shell-derived activated carbons and the effective micropores at different temperatures. *Chem Eng J* [Internet]. 2014 Oct 1;253:46–54. Available from: [<URL>](#).

101. Zhu X-L, Wang P-Y, Peng C, Yang J, Yan X-B. Activated carbon produced from paulownia sawdust for high-performance CO<sub>2</sub> sorbents. *Chinese Chem Lett* [Internet]. 2014 Jun 1;25(6):929–32. Available from: [<URL>](#).
102. Plaza MG, González AS, Pevida C, Pis JJ, Rubiera F. Valorisation of spent coffee grounds as CO<sub>2</sub> adsorbents for postcombustion capture applications. *Appl Energy* [Internet]. 2012 Nov 1;99:272–9. Available from: [<URL>](#).
103. Delgado LF, Charles P, Glucina K, Morlay C. The removal of endocrine disrupting compounds, pharmaceutically activated compounds and cyanobacterial toxins during drinking water preparation using activated carbon—A review. *Sci Total Environ* [Internet]. 2012 Oct 1;435–436:509–25. Available from: [<URL>](#).
104. Libbrecht W, Verberckmoes A, Thybaut JW, Van Der Voort P, De Clercq J. Soft templated mesoporous carbons: Tuning the porosity for the adsorption of large organic pollutants. *Carbon N Y* [Internet]. 2017 May 1;116:528–46. Available from: [<URL>](#).
105. Danish M, Ahmad T. A review on utilization of wood biomass as a sustainable precursor for activated carbon production and application. *Renew Sustain Energy Rev* [Internet]. 2018 May 1;87:1–21. Available from: [<URL>](#).
106. Jawad AH, Saud Abdulhameed A, Wilson LD, Syed-Hassan SSA, ALOthman ZA, Rizwan Khan M. High surface area and mesoporous activated carbon from KOH-activated dragon fruit peels for methylene blue dye adsorption: Optimization and mechanism study. *Chinese J Chem Eng* [Internet]. 2021 Apr 1;32:281–90. Available from: [<URL>](#).
107. Brito MJP, Veloso CM, Santos LS, Bonomo RCF, Fontan R da CI. Adsorption of the textile dye Dianix® royal blue CC onto carbons obtained from yellow mombin fruit stones and activated with KOH and H<sub>3</sub>PO<sub>4</sub>: kinetics, adsorption equilibrium and thermodynamic studies. *Powder Technol* [Internet]. 2018 Nov 1;339:334–43. Available from: [<URL>](#).
108. Sangon S, Hunt AJ, Attard TM, Mengchang P, Ngernyen Y, Supanchaiyamat N. Valorisation of waste rice straw for the production of highly effective carbon based adsorbents for dyes removal. *J Clean Prod* [Internet]. 2018 Jan 20;172:1128–39. Available from: [<URL>](#).
109. El-Bery HM, Saleh M, El-Gendy RA, Saleh MR, Thabet SM. High adsorption capacity of phenol and methylene blue using activated carbon derived from lignocellulosic agriculture wastes. *Sci Rep* [Internet]. 2022 Mar 31;12(1):5499. Available from: [<URL>](#).
110. Abbaci F, Nait-Merzoug A, Guellati O, Harat A, El Haskouri J, Delhalle J, et al. Bio/KOH ratio effect on activated biochar and their dye based wastewater depollution. *J Anal Appl Pyrolysis* [Internet]. 2022 Mar 1;162:105452. Available from: [<URL>](#).
111. Sun J, Ji L, Han X, Wu Z, Cai L, Guo J, et al. Mesoporous Activated Biochar from Crab Shell with Enhanced Adsorption Performance for Tetracycline. *Foods* [Internet]. 2023 Mar 1;12(5):1042. Available from: [<URL>](#).
112. Balathanigaimani MS, Shim W-G, Lee M-J, Kim C, Lee J-W, Moon H. Highly porous electrodes from novel corn grains-based activated carbons for electrical double layer capacitors. *Electrochem Commun* [Internet]. 2008 Jun 1;10(6):868–71. Available from: [<URL>](#).
113. Wu Y, Cao J-P, Zhuang Q-Q, Zhao X-Y, Zhou Z, Wei Y-L, et al. Biomass-derived three-dimensional hierarchical porous carbon network for symmetric supercapacitors with ultra-high energy density in ionic liquid electrolyte. *Electrochim Acta* [Internet]. 2021 Mar 1;371:137825. Available from: [<URL>](#).
114. Karnan M, Subramani K, Srividhya PK, Sathish M. Electrochemical Studies on Corncob Derived Activated Porous Carbon for Supercapacitors Application in Aqueous and Non-aqueous Electrolytes. *Electrochim Acta* [Internet]. 2017 Feb 20;228:586–96. Available from: [<URL>](#).
115. Ponce MF, Mamani A, Jerez F, Castilla J, Ramos PB, Acosta GG, et al. Activated carbon from olive tree pruning residue for symmetric solid-state supercapacitor. *Energy* [Internet]. 2022 Dec 1;260:125092. Available from: [<URL>](#).
116. Enock TK, King'ondeu CK, Pogrebnoi A, Jande YAC. Biogas-slurry derived mesoporous carbon for supercapacitor applications. *Mater Today Energy* [Internet]. 2017 Sep 1;5:126–37. Available from: [<URL>](#).
117. Zou Z, Luo X, Wang L, Zhang Y, Xu Z, Jiang C. Highly mesoporous carbons derived from corn silks as high performance electrode materials of supercapacitors and zinc ion capacitors. *J Energy Storage* [Internet]. 2021 Dec 1;44:103385. Available from: [<URL>](#).